

Predicting Joint Torque from Spike Trains


Harmen Siezen, Antonio Gogeochea, Arnoud Visser, Bardia Rodd, Massimo Sartori,
Utku Şükrü Yavuz


Proc. MIT Undergraduate Research Technology Conference (URTC), October 10–12, 2025, Cambridge,
MA


Author's accepted manuscript preprint.


Final version of record available from IEEE Xplore (DOI: *to be added*).


Predicting Joint Torque from Spike Trains


Harmen Siezen 
Faculty of Science
University of Amsterdam
Amsterdam, The Netherlands
0009-0003-6553-3967

Dr.ir. Antonio Gogeaşcoechea 
Dept. of Biomechanical Engineering
University of Twente
Enschede, The Netherlands
0000-0003-0553-897X

Dr. Arnoud Visser 
Informatics Institute, Faculty of Science
University of Amsterdam
Amsterdam, The Netherlands
0000-0002-7525-7017

Dr. Bardia Rodd 
The State University of New York
SUNY Upstate Medical University
Syracuse, NY 13210 USA
0000-0003-3121-7045

Dr. Massimo Sartori 
Dept. of Biomechanical Engineering
University of Twente
Enschede, The Netherlands
0000-0003-0930-6535

Dr. Utku S. Yavuz 
Dept. of Biomedical Signals and Systems
University of Twente
Enschede, The Netherlands
0000-0002-6968-8064

Abstract—The development of human-machine interfaces is key to creating prosthetics that adapt to user intent. However, there remains much incongruity between muscle activity and the resulting torque. This study employs high-density surface electromyography (HD-sEMG) in conjunction with the Fast-ICA algorithm to decompose motor units (MUs), which play a crucial role in the generation of movement. Multilayer perceptron (MLP) architectures are evaluated for predicting joint torque from MU activity, and transfer learning is explored to enhance training performance. Results show that transfer learning enhances training efficiency and that joint torque can be accurately predicted from MU activity, thereby advancing the potential of control systems in assistive technologies.

Index Terms—High-Density Surface Electromyography (HD-sEMG), Motor Unit Decomposition, Multilayer Perceptron (MLP), Machine Learning, Signal Processing, Transfer Learning, Joint Torque Prediction

I. INTRODUCTION

An estimated 2.3 million individuals in the United States are currently living with limb loss, a number projected to increase by 145% by 2060 [1], [2]. Approximately 86% of all amputations globally are lower-limb amputations [3]. This growing population of lower-limb amputees underscores the urgent need for effective medical solutions. One promising approach is the use of prosthetic devices, which aim to restore lost human function following amputation [4]. Despite their potential, current prosthetics have limited effectiveness, primarily due to the limited understanding of human-prosthesis interactions, which hinders the development of devices capable of adapting intuitively to user intent [5].

Research suggests that the ability of prosthetics to restore human function largely depends on their ability to interface with the central nervous system (CNS) [6]. The CNS, consisting of the brain and spinal cord, controls muscles through motor units. Each MU consists of a motor neuron, located in the spinal cord, and all the muscle fibers it innervates. Muscle activation is regulated by a pool of motor neurons; therefore, multiple MUs coordinate to control each muscle [7]. The activation of an MU causes all the muscle fibers it controls

to contract simultaneously. This muscle contraction generates force and joint torque, which then produces movement [2], [8].

The firing of muscle fibers generates electrical activity that can be detected on the skin surface using electrodes, which is a process known as surface electromyography (sEMG). Each time a MU fires, it produces a characteristic waveform called a motor unit action potential (MUAP), which reflects the summed electrical activity of the muscle fibers innervated by that MU. However, since multiple MUs fire simultaneously, the electrical signals recorded by sEMG often overlap, making it difficult to determine which signal originates from which MU [9]. To address this, high-density surface electromyography is employed, which involves placing an array of closely spaced electrodes over the muscle surface [10]. By leveraging spatial information from multiple electrode channels, signal decomposition techniques can be applied to isolate and identify activity of individual MUs [11].

With the use of machine learning algorithms, complex patterns can be captured in decomposed MU signals, enabling the prediction of joint torque based on MU activity [12], [13]. While substantial research has focused on upper-limb prosthetics [14], the majority of amputations are lower-limb, motivating this paper's focus on investigating HD-sEMG signals recorded from leg muscles in relation to joint torque.

Much of the existing work frames this problem as a classification task, predicting discrete movements [12], [13]. However, human movement is highly dynamic, which limits the generalizability of such class-based models to novel or transitional actions [15]–[17]. Therefore, this work approaches this as a regression task, where torque is modeled as a continuous function of MU activation recorded per muscle.

To predict torque, a multilayer perceptron is employed for its ability to model continuous outputs, unlike previous studies that used linear discriminant analysis and support vector machines, which are limited to discrete class predictions [18]. This enables adaptation to scenarios that are not class-specific, expanding the model's predictive range beyond predefined

categories. Deep neural networks, such as convolutional neural networks, are prone to overfitting on small, subject-specific datasets [19]. In contrast, the simpler architecture of the MLP allows for accurate prediction with a relatively small number of parameters, improving training efficiency and reducing the risk of overfitting. Prior work has shown that MLPs can achieve high accuracy on multiclass problems; for example, reaching up to 82% accuracy on a 12-class problem [20]. This demonstrates their capacity to learn complex decision boundaries, which is promising for regression tasks requiring continuous value prediction.

In addition, patient data is often limited, restricting the amount of training data available for machine learning algorithms and potentially hindering performance [19]. To address this, the proposed methodology incorporates transfer learning to assess its ability to compensate for limited patient-specific data. Transfer learning reduces data requirements by leveraging parameters previously learned from large datasets [21]. This approach enhances the applicability of neural-based lower leg prosthetics, enabling models controlling these devices to adapt to new users with improved training efficiency.

II. METHOD

This paper proposes a framework to predict joint torque based on HD-sEMG signals recorded from multiple muscles on the right leg of three subjects. To assess transfer learning, models are first pretrained on data from one subject and then evaluated on another subject to determine whether transfer learning improves performance.

A. Data Collection

All experimental procedures were approved by the University Medical Center Göttingen Ethical Committee (Ethikkommission der Universitätsmedizin Göttingen, approval number 01/10/12). After providing signed informed consent, data were collected from four healthy men (weight: 68.3 ± 1.3 kg, age: 30 ± 1.9 years, height: 184 ± 2.1 cm) who volunteered for this investigation [4], [22]. The data from one of these subjects was excluded due to a task mismatch; therefore, the data from only three subjects were used [2].

Muscle activity and joint angular moments were recorded simultaneously at 2048 Hz from the subject's right leg. Ankle torque was measured using a dynamometer (M3, Biodex, Medical Systems Inc., Shirley, NY, USA). HD-sEMG signals were acquired using a 256-channel surface EMG system (EMG-USB2, OT Bioelettronica, Torino, Italy). Recordings were obtained from the subject's right lower leg muscles using two 32-channel grids and three 64-channel grids, each with 10 mm inter-electrode distance [2], [4].

The two 32-channel grids were applied to the gastrocnemius lateralis (GL) and the peroneus group, which is split into the peroneus tertius (PT) (active during dorsiflexion) and the peroneus longus (PL) (active during plantarflexion). The three 64-channel grids were used for the tibialis anterior (TA), soleus (SOL), and gastrocnemius medialis (GM) muscles (see Fig. 1). Prior to electrode placement, the skin was shaved and lightly

abraded. Electrodes were applied to the skin using conductive paste and secured with 1 mm-thick double-adhesive foam with holes corresponding to each sensing site [2], [4], [17].

B. Experimental Protocol

The subjects performed a series of isometric dorsiflexion and plantarflexion contractions, moving the ankle from rest to target force levels expressed as percentages of maximum voluntary contraction (MVC) in either dorsiflexion or plantarflexion. The protocol included four target levels: 30%, 50%, 70%, and 90% of MVC [2], [4], [17].

C. Signal Preprocessing

A simplification of the HD-sEMG generation model [23] is the linear instantaneous mixing model, in which the HD-sEMG recordings are modeled as a linear mixture of the sources:

$$x(k) = As(k) \quad (1)$$

where A is an unknown mixing matrix, $x(k)$ represents the observed HD-sEMG recordings, and $s(k)$ are the source signals corresponding to the motor unit spike trains, which represent action potentials generated by individual motor units. The variable $k \in \{1, \dots, D\}$ represents the sample index [2], [8], [10].

The HD-sEMG signals are high-pass filtered with a 30 Hz cut-off frequency to eliminate movement artifacts [4]. The filtered signals are then whitened and extended using an extension factor of 16, which has been shown to yield optimal results [10]. Extending the signals introduces time-lagged versions of each channel to promote statistical independence between sources. This preprocessing enables the source extraction via a blind source separation method, which models the sources as:

$$s(k) = Wz(k) \quad (2)$$

where the sources $s(k)$ are a linear combination of the extended whitened observation $z(k)$ and W is obtained using the FAST-ICA algorithm [11] such that $W \approx A^{-1}$ [2], [8], [10].

The recorded torque moments are low-pass filtered with 2 Hz cut-off frequency to remove high-frequency noise [4]. Moments are then averaged over a 5-s time window during which the subjects exert no torque. This average is used to

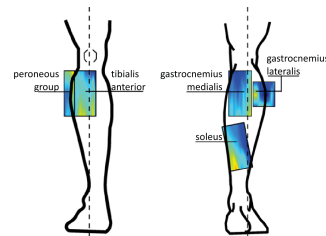


Fig. 1: Placement of high-density sEMG grid electrodes on lower leg muscles, including the soleus, gastrocnemius, tibialis anterior, and peroneus muscles. Adapted from [4].

remove the torque offset from the recorded moments caused by the weight of the subject's leg [2], [4].

D. Feature Extraction

The estimated sources $s(k)$ are used to predict torque using an MLP. However, since the number of extracted sources can vary per muscle [17], the sources are aggregated per muscle:

$$s_m(k) = \sum_{j=1}^{n_m} s_{j,m}(k) \quad (3)$$

where n_m denotes the number of estimated sources for muscle m , with $m \in M = \{\text{TA, SOL, GM, GL, PL, PT}\}$. This summation produces a single source signal per muscle, $s_m(k)$, resulting in a feature vector of size 6 corresponding to the six recorded muscles. This allows for a consistent input format to the MLP model.

Next, the summed sources per muscle are transformed into muscle-specific feature functions by applying a twitch contraction model, which predicts muscle activation based on the sources:

$$f_m(k) = \left(2 \cdot \exp^{-\frac{T}{t_{\text{peak}}}} \right) \cdot f(k-1) - \left(\exp^{-\frac{(-2 \cdot T)}{t_{\text{peak}}}} \right) \cdot f(k-2) + \frac{(A_{\text{peak}} \cdot T^2)}{t_{\text{peak}}} \cdot \exp^{1-\frac{T}{t_{\text{peak}}}} \cdot s_m(k-1) \quad (4)$$

where A_{peak} is the peak, and t_{peak} is the time to peak (or contraction time) of the twitch. $f_m(k)$ models the muscle activation generated by the summed sources $s_m(k-1)$, and T denotes the sampling period (time between samples), $T = \frac{1}{2024}$ [17], [24]. This results in a muscle-specific feature function. For this paper, values 0.1 were used for both A_{peak} and t_{peak} , aligning with previous research on twitch functions [17].

The 6 muscle-specific feature functions are used as input to the MLP. Based on these features, the MLP predicts the low-pass filtered torque for each subject, performing a specific movement type at a specific MVC level (See Section II-B):

$$\text{Torque}(k) \approx \text{MLP}(f_M(k)), \text{ where } f_M(k) = \begin{bmatrix} f_{\text{TA}}(k) \\ f_{\text{SOL}}(k) \\ f_{\text{GM}}(k) \\ f_{\text{GL}}(k) \\ f_{\text{PL}}(k) \\ f_{\text{PT}}(k) \end{bmatrix} \quad (5)$$

Different MLP architectures are tested with 3, 5, and 9 layers, each containing 8, 16, or 32 nodes, as these configurations have demonstrated high predictive accuracy in previous studies [25], [26]. Following established practices in related work, the learning rate is set to 0.0009, and training is conducted for 500 epochs [27].

E. Time Series Cross-Validation

Time series cross-validation is used to evaluate the model's ability to predict torque while fully respecting the temporal order of the data, thereby preventing unrealistic data leakage that would occur if future observations were used to predict the past. To avoid such leakage across training and test sets, the continuous signal is divided into four discrete blocks corresponding to individual contractions. For each fold, the model is trained on all blocks up to a certain block, and tested on the subsequent block, resulting in three folds: fold 1 trains on block 1 and tests on block 2, fold 2 trains on blocks 1 and 2 and tests on block 3, and fold 3 trains on blocks 1 to 3 and tests on block 4 (See Fig. 3a). This ensures that information from future contractions does not appear in the training data [28], [29].

F. Transfer Learning

To investigate the effect of transfer learning, the performance of multiple baseline MLPs is compared to that of pretrained MLPs. Each pretrained model is initially trained on data from one subject performing a specific movement and then fine-tuned on data from only block 1 (a smaller portion of data) and tested on block 4 (See Fig. 4b) from the target subject performing the same movement. The baseline model is trained and tested on blocks 1 and 4, respectively, from the target subject. This setup evaluates whether pertaining reduces the amount of subject-specific data required for accurate prediction. To ensure fair comparison, each subject is used once as the pretraining source and once as the fine-tuning target for every combination of movement type and MVC level. Final results are averaged across all subject pairs and conditions.

To assess training efficiency, the training loss curves are compared between pretrained and baseline models. To assess data efficiency, the test loss of pretrained models is compared to that of baseline models when trained on reduced amounts of data.

III. RESULTS

The first step was to obtain the raw EMG and torque recordings (see Figs. 4a and 2a). The surface EMG recordings were decomposed into spike trains using the Fast-ICA algorithm [11] and subsequently summed, as illustrated in Fig. 4b. These summed spike trains were then used to derive muscle-specific feature functions $f_m(k)$, as shown in Fig. 4c. Each raw torque measurement contained a baseline offset, which was estimated using the first 5 seconds of data (indicated by the orange band in Fig. 2b). The torque signals were then filtered and corrected for this offset as shown in Fig. 2c.

Different MLP architectures were evaluated using features extracted from subject 1 during a dorsiflexion task at 30% MVC, employing 3-fold time series cross-validation. Experiments were conducted to determine the optimal width and number of hidden layers. The best-performing architecture consisted of five hidden layers with 32 nodes each (See Table I). The table shows that increasing the number of

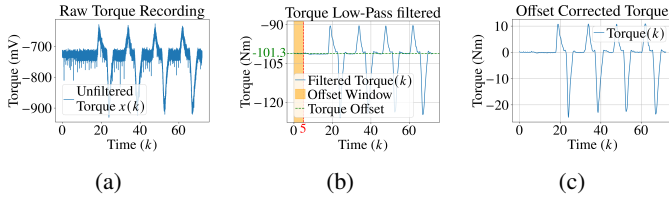


Fig. 2: (a) Raw torque recordings from subject 1 performing four repeated movements at 30% MVC. these raw measurements are smoothed with a low-pass filter (b), and offset corrected such that the baseline has a torque of 0.0 Nm (c).

TABLE I: Average 3-fold time series cross-validation loss (mean squared error) for MLP architectures trained and tested on subject 1, performing a dorsiflexion movement at 30% MVC. The architectures used a consistent number of nodes per hidden layer.

Hidden Layers	Width 8	Width 16	Width 32
3	0.82	0.78	0.76
5	0.81	0.75	0.72
9	0.77	0.79	0.72

nodes per layer reduces mean squared error (MSE), while increasing the number of layers has minimal effect. All tested architectures used a consistent number of nodes per hidden layer; for example, an MLP with five hidden layers and width 8 corresponds to the structure $MLP_{6 \times 8 \times 8 \times 8 \times 8 \times 1}$.

The MLP architecture, comprising 5 hidden layers with 32 nodes per layer, was able to accurately predict the shape of the filtered torque curve, as illustrated in Fig. 5.

The same MLP architecture was used to evaluate improvements in training and data efficiency through transfer learning. As shown in Fig. 6b, pretrained models reached the same MSE in fewer epochs across all MVC levels compared to the baseline models, indicating reduced computational cost. Additionally, Fig. 6a shows that the average MSE increased with MVC level for both the pretrained and baseline models. This

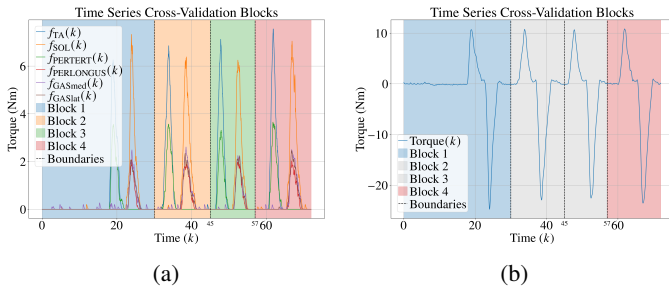


Fig. 3: (a) Muscle-specific feature functions from six different muscle groups, and (b) filtered torque recordings from subject 1 performing four repeated movements at 30% MVC. These repeated movements are collected in four blocks, each including both EMG recordings and corresponding torque measurements, which are used for time-series cross-validation and transfer learning assessments.

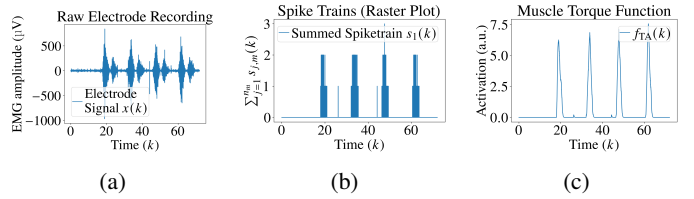


Fig. 4: (a) Raw EMG recordings from subject 1 performing four repeated dorsiflexion movements at 30% MVC, recorded from the first electrode over the tibialis anterior muscle. These raw measurements are aggregated into spike trains (b), which are turned into muscle-specific feature functions (c).

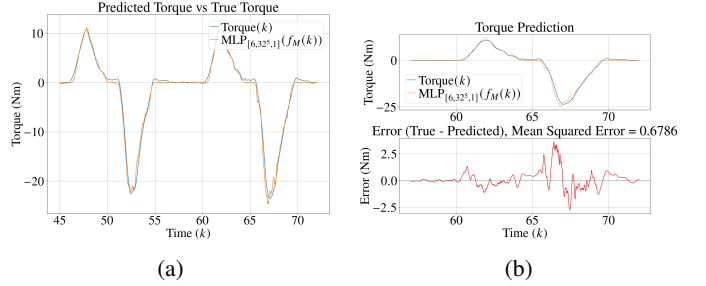


Fig. 5: Torque predictions made by the multilayer perceptron ($MLP_{6 \times 32 \times 32 \times 32 \times 32 \times 1}$) after training on the first two blocks (45 seconds) of subject 1 performing a dorsiflexion movement at 30% MVC. (a) Shows both the predicted and actual torque curves, while (b) zooms in on block 4, highlighting the largest remaining error occurring during the sharp decline around 66.0 seconds.

trend likely stems from the increased complexity of the HD-sEMG signal at higher force levels [30]. Greater force recruits more MUs, causing more overlapping action potentials that hinder MU identification and may reduce model accuracy [7], [9], [31]. However, pretrained models showed marginal, if any, improvements in test accuracy. This observation aligns with prior findings that transfer learning tends to be less effective for tasks involving simpler or lower-dimensional input data, where the complexity of learned feature representations offers limited benefit [19], [32].

Compared to state-of-the-art musculoskeletal approaches on the same dataset (reported normalized RMSEs <0.4 in Massimo et al. [4] and <0.3 in Gogea-scoeche et al. [17]), Fig. 5 shows peak errors below 4 Nm on a 23.5 Nm contraction, over which we calculated a normalized RMSE of 0.154. While this is only an illustrative example for a single subject at 30% MVC, it highlights the potential of the proposed approach.

IV. CONCLUSION

The results show that increasing the number of nodes per hidden layer in MLP architectures improves prediction accuracy, while the number of hidden layers has minimal impact. Transfer learning provides marginal gains in data efficiency but significantly reduces training time compared to MLPs trained from scratch. This improvement enhances the applicability of

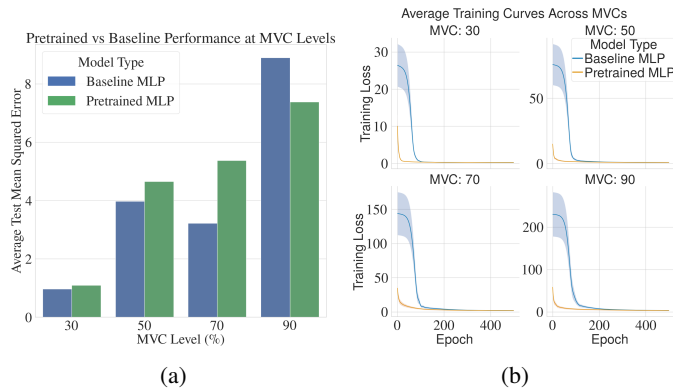


Fig. 6: Training loss curves (mean squared error \pm standard error of the mean) and average test loss (mean squared error) for pretrained and baseline MLPs. (a) Bars represent the average test loss across all subject pairs performing the same movement type at the same MVC level. (b) Plots show average training loss across subject pairs performing the same movement type at the same MVC level.

MLP-driven prosthetics in scenarios with limited computational resources, suggesting that EMG-driven prosthetics could benefit from shared learned parameters across users. Overall, this approach enables accurate torque prediction by interfacing with the nervous system, supporting the development of leg prostheses that adapt to user intent.

V. ACKNOWLEDGMENTS

This work received no external funding, and the authors declare no competing personal interests.

REFERENCES

- [1] J. A. Rivera, K. Churovich, A. B. Anderson, and B. K. Potter, "Estimating Recent US Limb Loss Prevalence and Updating Future Projections," *Archives of Rehabilitation Research and Clinical Translation*, vol. 6, no. 4, p. 100376, 2024.
- [2] H. Siezen, "MLP-Based Torque Estimation from Decomposed HD-sEMG Signals," Bachelor's Thesis, University of Amsterdam, 2025.
- [3] Amputee Coalition and Avalere Health, "Prevalence of Limb Loss and Limb Difference in the United States: Implications for Public Policy," Amputee Coalition, White Paper, Feb. 2024, based on Avalere Health analysis of insurance claims data.
- [4] M. Sartori, U. Yavuz, and D. Farina, "In Vivo Neuromechanics: Decoding Causal Motor Neuron Behavior with Resulting Musculoskeletal Function," *Scientific Reports*, vol. 7, no. 13465, Oct 2017.
- [5] Ł. Kidziński, C. Ong, S. P. Mohanty, J. Hicks, S. Carroll, B. Zhou *et al.*, "Artificial intelligence for prosthetics: Challenge solutions," in *The NeurIPS'18 Competition: From Machine Learning to Intelligent Conversations*. Springer, 2020, pp. 69–128.
- [6] R. Ornelas-Kobayashi, R. Mooiweer, and M. Sartori, "Towards Personalized Motor-Restoring Technologies: Characterizing Neural Data-Driven Alpha-Motoneuron Model Parameters," in *2024 10th IEEE RAS/EMBS International Conference for Biomedical Robotics and Biomechatronics (BioRob)*. IEEE, 2024, pp. 1581–1586.
- [7] M. Carbonaro, "Detecting neuromechanical properties of single motor unit by combining high-density electromyography and ultrafast ultrasonography," Ph.D. Thesis, University of Turin, 2023.
- [8] B. van Dieren, "Decoding motor unit firing events during walking : An adaptive approach validated with intramuscular electromyography," Master's Thesis, University of Twente, March 2025.
- [9] R. Merletti, *Electromyography: Physiology, Engineering, and Non-Invasive Applications*. Hoboken, NJ: Wiley, Aug 2004.
- [10] M. Talke, "Using Supervised Deep Learning for Real-Time Motor Unit Decomposition of High-Density Surface Electromyography Signals," Master's Thesis, Aalto University, Espoo, Finland, Jun 2022.
- [11] F. Negro, S. Muceli, A. M. Castronovo, A. Holobar, and D. Farina, "Multi-channel intramuscular and surface EMG decomposition by convolutive blind source separation," *Journal of Neural Engineering*, vol. 13, no. 2, p. 026027, 2016.
- [12] S. Krishnapriya, J. P. Sahoo, and S. Ari, "Surface electromyography based hand gesture signal classification using 1d cnn," in *2023 International Conference on Intelligent Systems, Advanced Computing and Communication (ISACC)*. IEEE, 2023, pp. 1–6.
- [13] D. K. Luu, A. T. Nguyen, M. Jiang, M. W. Drealan, J. Xu, T. Wu, W.-k. Tam, W. Zhao, B. Z. Lim, C. K. Overstreet *et al.*, "Artificial intelligence enables real-time and intuitive control of prostheses via nerve interface," *IEEE Transactions on Biomedical Engineering*, vol. 69, no. 10, pp. 3051–3063, 2022.
- [14] N. Jiang, C. Chen, J. He, J. Meng, L. Pan, S. Su, and X. Zhu, "Bio-robotics research for non-invasive myoelectric neural interfaces for upper-limb prosthetic control: a 10-year perspective review," *National Science Review*, vol. 10, no. 5, p. nwad048, Feb 2023.
- [15] L. P. Leahy, "Estimating output torque via amplitude estimation and neural drive: a high-density sEMG study," Master's Thesis, Massachusetts Institute of Technology, Department of Mechanical Engineering, 2020.
- [16] D. Farina, I. Vujaklija, M. Sartori, T. Kapelner, F. Negro, N. Jiang *et al.*, "Man/machine interface based on the discharge timings of spinal motor neurons after targeted muscle reinnervation," *Nature Biomedical Engineering*, vol. 1, no. 2, p. 0025, 2017.
- [17] A. Gogeaocoechea, R. Ornelas-Kobayashi, U. S. Yavuz, and M. Sartori, "Characterization of motor unit firing and twitch properties for decoding musculoskeletal force in the human ankle joint in vivo," *IEEE Transactions on Neural Systems and Rehabilitation Engineering*, vol. 31, pp. 4040–4050, 2023.
- [18] A. Alkan and M. Günay, "Identification of EMG signals using discriminant analysis and SVM classifier," *Expert Systems with Applications*, vol. 39, no. 1, pp. 44–47, 2012.
- [19] I. Goodfellow, Y. Bengio, and A. Courville, *Deep Learning*. Cambridge, MA: MIT Press, 2016.
- [20] W. Geng, Y. Du, W. Jin, W. Wei, Y. Hu, and J. Li, "Gesture recognition by instantaneous surface EMG images," *Scientific Reports*, vol. 6, no. 1, p. 36571, 2016.
- [21] N. Rieke, J. Hancox, W. Li, F. Milletari, H. Roth, S. Albarqouni, S. Bakas *et al.*, "The future of digital health with federated learning," *npj Digital Medicine*, vol. 3, Dec 2020.
- [22] World Medical Association, "World Medical Association Declaration of Helsinki: Ethical principles for medical research involving human subjects," *JAMA*, vol. 310, no. 20, pp. 2191–2194, 2013.
- [23] A. Holobar and D. Zazula, "Multichannel blind source separation using convolution kernel compensation," *IEEE Transactions on Signal Processing*, vol. 55, no. 9, pp. 4487–4496, 2007.
- [24] R. Cisi and A. Kohn, "Simulation system of spinal cord motor nuclei and associated nerves and muscles, in a web-based architecture," *Journal of Computational Neuroscience*, vol. 25, pp. 520–542, Jun 2008.
- [25] H. Ziai and C. Menon, "Comparison of regression models for estimation of isometric wrist joint torques using surface electromyography," *Journal of NeuroEngineering and Rehabilitation*, vol. 8, p. 56, 2011.
- [26] J. An and I. Lee, "Artificial neural network-based ground reaction force estimation and learning for dynamic-legged robot systems," *PeerJ Computer Science*, 2023.
- [27] L. Zhang, Z. Li, Y. Hu, C. Smith, E. M. G. Farewik, and R. Wang, "Ankle Joint Torque Estimation Using an EMG-Driven Neuromusculoskeletal Model and an Artificial Neural Network Model," *IEEE Transactions on Automation Science and Engineering*, vol. 18, no. 2, pp. 564–573, 2021.
- [28] J. Yang, M. Soh, V. Lieu, D. J. Weber, and Z. Erickson, "EMGBench: Benchmarking Out-of-Distribution Generalization and Adaptation for Electromyography," *arXiv preprint arXiv:2410.23625*, 2024.
- [29] R. J. Hyndman and G. Athanasopoulos, *Forecasting: principles and practice*, 3rd ed. Melbourne, Australia: OTexts, 2021.
- [30] E. Henneman, "Relation between size of neurons and their susceptibility to discharge," *Science*, vol. 126, no. 3287, pp. 1345–1347, 1957.
- [31] M. Chen and P. Zhou, "High-density surface emg decomposition: Achievements, challenges, and concerns," *IEEE Transactions on Neural Systems and Rehabilitation Engineering*, vol. 33, pp. 1212–1219, 2025.
- [32] S. Kornblith, J. Shlens, and Q. V. Le, "Do better imagenet models transfer better?" *arXiv preprint arXiv:1805.08974*, 2019.